

Trion-mediated Förster resonance energy transfer and optical gating effect in WS₂/hBN/MoSe₂ heterojunction

Hu, Zehua; Hernández-Martínez, Pedro Ludwig; Liu, Xue; Amara, Mohamed-Raouf; Zhao, Weijie; Watanabe, Kenji; Taniguchi, Takashi; Demir, Hilmi Volkan; Xiong, Qihua

2020

Hu, Z., Hernandez-Martinez, P. L., Liu, X., Amara, M.-R., Zhao, W., Watanabe, K., ... Xiong, Q. (2020). Trion-mediated Förster resonance energy transfer and optical gating effect in WS₂/hBN/MoSe₂ heterojunction. *ACS Nano*, 14(10), 13470–13477.
doi:10.1021/acsnano.0c05447

<https://hdl.handle.net/10356/144347>

<https://doi.org/10.1021/acsnano.0c05447>

This document is the Accepted Manuscript version of a Published Work that appeared in final form in *ACS Nano*, copyright © American Chemical Society after peer review and technical editing by the publisher. To access the final edited and published work see <https://doi.org/>

Downloaded on 06 Dec 2022 18:48:50 SGT

Trion-Mediated Förster Resonance Energy Transfer and Optical Gating Effect in
WS₂/hBN/MoSe₂ Heterojunction

Zehua Hu[†], Pedro Ludwig Hernández-Martínez[‡], Xue Liu[†], Mohamed-Raouf Amara[†], Weijie Zhao[†],
Kenji Watanabe[§], Takashi Taniguchi[§], Hilmi Volkan Demir^{‡, ⊥}, Qihua Xiong^{*, †, ⊥}

[†]Division of Physics and Applied Physics, School of Physical and Mathematical Sciences, Nanyang
Technological University, 637371, Singapore

[‡]LUMINOUS! Center of Excellence for Semiconductor Lighting and Display, School of Electrical
and Electronics Engineering, Nanyang Technological University, Singapore 639798, Singapore

[§]Advanced Materials Laboratory, National Institute for Materials Science, 1-1 Namiki, Tsukuba,
305-0044, Japan

[⊥]Department of Physics, Department of Electrical and Electronics Engineering, UNAM-National
Nanotechnology Research Center and Institute of Materials Science and Nanotechnology, Bilkent
University, Ankara 06800, Turkey

[⊥]State Key Laboratory of Low-Dimensional Quantum Physics, Department of Physics, Tsinghua
University, Beijing 100084, China.

*Corresponding author. E-mail: qihua@ntu.edu.sg

Abstract

Van der Waals two-dimensional layered heterostructures have recently emerged as a platform, where the interlayer couplings give rise to interesting physics and multifunctionalities in optoelectronics. Such couplings can be rationally controlled by dielectric, separation, and stacking angles, which affect the overall charge or energy transfer processes, and emergent potential landscape for twistrionics. Herein, we report the efficient Förster resonance energy transfer (FRET) in WS₂/hBN/MoSe₂ heterostructure, probed by both steady-state and time-resolved optical spectroscopy. We clarified the evolution behavior of the electron-hole pairs and free electrons from the trions, *i.e.*, ~59.9% of the electron-hole pairs could transfer into MoSe₂ by FRET channels (~38 ps) while the free electrons accumulate at the WS₂/hBN interface to photogate MoSe₂. This study presents a clear picture of the FRET process in two-dimensional transition metal dichalcogenides heterojunctions, which establishes the scientific foundation for developing the related heterojunction optoelectronic devices.

Keywords: 2D materials, transition metal dichalcogenides, trion, van der Waals heterostructure, Förster resonance energy transfer, photogating, optical spectroscopy,

Energy transfer refers to the nonradiative transfer of an electronic excitation from a donor to an acceptor. This process avoids the emission and reabsorption events, thus possessing a high energy conversion efficiency.¹ Energy transfer can be divided into Dexter and Förster type, whereas the former is based on electron exchange thus only works in the close proximity (<1 nm); while the latter depends on dipole-dipole coupling and works in a relatively long distance (r) with a $1/r^6$ dependence in the molecular dye system.^{2,3} During the past three decades, Förster resonance energy transfer (FRET) has been intensively studied for various important optoelectronic applications including solar cell,⁴ light-emitting diode,⁵ and laser.⁶ Such applications in optoelectronics are highly compatible with recently emerged two-dimensional (2D) van der Waals materials. Due to the reduced dimension and strong confinement in the 2D limit, the dipole-dipole coupling strength is proportional to $1/r^4$, rather than $1/r^6$ in 3D confinement, enabling a stronger interaction strength and more pronounced long-range characteristics.^{7,8}

2D materials such as graphene, hexagonal boron nitride (h-BN) and transition metal dichalcogenides (TMDs) offer a platform to study fundamental physics in a single atomic layer limit.^{9, 10} Monolayer TMDs hold high stability and sizeable direct bandgap covering from visible to near-infrared spectrum. Due to the reduced dielectric screening effect, monolayer TMDs feature strong excitonic emission even at room temperature with a binding energy of several hundred meV.¹¹ Many-body effect of the excitonic species is strong and highly sensitive to the doping level, allowing the characterization and manipulation of trions or even biexcitons.^{12, 13} Inversion symmetry breaking and strong spin-orbit coupling enable more exciting physics, including valleytronics and spin-forbidden dark states.^{14, 15} Since monolayer TMD heterojunctions usually form type II band alignment, optically excited electrons and holes are readily separated and then accumulate in the opposite monolayers. Pump-probe method has proven such charge transfer process in the heterostructure to be ultrafast (~ 100 fs).¹⁶⁻²¹ The appropriate material combination and careful stacking, *e.g.*, MoSe₂ and WSe₂, can form strong interlayer exciton with long lifetime and novel valleytronic properties.^{22, 23} Besides charge transfer, energy transfer is another important interaction between semiconducting emitters, which are widely studied in quantum dots and organic molecules but much less in 2D material heterojunctions.²⁴⁻³⁰ Recently, by performing photoluminescence excitation (PLE) spectroscopy, FRET has been demonstrated in type II MoSe₂/WS₂ heterojunction.³¹ On the contrary, energy transfer at MoTe₂/WSe₂ interface is demonstrated to be Dexter type by pump-probe method, thus both direct and indirect exciton from the donor could transfer and contribute to the acceptor emission.³² Although FRET has been achieved in 2D material heterojunctions, it is simply attributed to a dipole-dipole coupling between excitons.^{31, 33} However, due to the reduced Coulomb screening effect and high intrinsic doping, 2D TMDs feature diverse emission species, including exciton, trion and even biexciton emission. The population and lifetime of different excitonic species are quite different, thus, one needs to be extremely careful when dealing with the dynamics in 2D TMD heterojunctions.^{12, 34, 35}

Here, we experimentally investigate the energy transfer process in WS₂/hBN/MoSe₂ heterojunction. By 532 nm (above WS₂ bandgap) excited photoluminescence (PL) mapping, we observe an enhancement of MoSe₂ exciton (X^0) emission, accompanied by the quenching of WS₂ trion (X^-)

emission. Such energy transfer occurs *via* a 3 nm hBN spacer, implying a clear signature of FRET. In combination with the shortening of WS_2 X^- PL lifetime, our study unambiguously reveals that FRET happens between X^- of WS_2 and X^0 of $MoSe_2$, *i.e.*, trion-exciton coupling owing to the strong coupling strength and a long intrinsic lifetime of X^- , rather than the direct exciton-exciton coupling proposed in literature.^{31, 33}

RESULTS AND DISCUSSION

All the heterojunctions are fabricated with standard stamp-assisted dry transfer method in the nitrogen-filled glovebox to minimize the influence from trapped moisture. After transfer, 5/60 nm chromium/gold electrodes are patterned by standard electron beam lithography process, followed by a high vacuum (10^{-6} mbar) annealing at 200 °C for 2 hours to enhance the interlayer coupling. All the optical spectroscopies presented in this paper are taken at 80 K in a liquid nitrogen-cooled cryostat unless otherwise stated.

Figure 1a shows the schematic structure and the optical image of the typical device. Here, monolayer WS_2 , ~3 nm thick hBN, and monolayer $MoSe_2$ are stacked layer by layer to form a heterojunction with distinct regions composing of: (I) $WS_2/hBN/MoSe_2$ (orange square in the sample image); (II) hBN/ $MoSe_2$ (green circle) and (III) WS_2/hBN . Therefore, the influence of WS_2 on the optical properties of $MoSe_2$ (or *vice versa*) can be qualitatively and quantitatively compared. Figure 1b-d illustrates the PL mapping data for $MoSe_2$ X^0 , X^- and X^0/X^- ratio excited by a 532 nm continuous-wave (CW) laser from the white dashed square in the bottom of Figure 1a. Compared to the case of $MoSe_2$ in region II, the $MoSe_2$ X^0 emission in the region I is enhanced by a factor of ~2.1 while the X^- emission is decreased by a factor of ~2/3 (Figure 1b, c), leading to a much higher $MoSe_2$ X^0/X^- ratio (Figure 1d), as reflected in the extracted PL spectra (Figure 1e). The changes of peak position and full width at half maximum (1.64 eV and 7 meV for X^0 ; 1.61 eV and 11 meV for X^-) are negligible due to nearly identical dielectric environment ($MoSe_2$ is sandwiched between SiO_2 and hBN). The enhancement of X^0 emission is attributed to the FRET from WS_2 as detailed later, while the X^- emission quenching results from the optical gating effect (p-doping) induced by the electron accumulation at the WS_2/hBN interface.

The optical gating scenario was confirmed by the Raman spectroscopy at the same position, which shows a small redshift of MoSe₂ A_{1g} mode by ~ 0.12 cm⁻¹ in the region I (Figure 1f, full-scale spectra is shown in Supplementary Figure 3a). As previously shown in literature, the A_{1g} mode of TMDs is sensitive to the doping level due to the strong electron-phonon coupling.³⁶ Hence, the small redshift here is the direct evidence of weak p-doping.³⁶ For WS₂, the PL is dominated by X⁻ emission. The stacking of hBN/MoSe₂ quenched the WS₂ X⁻ emission intensity by almost half, suggesting the exciton energy transfer from WS₂ X⁻ to MoSe₂ X⁰ (Figure 1e).

Then, the excitation wavelength was tuned to 671 nm, *i.e.*, below WS₂ bandgap excitation (Supplementary Figures 1, 4). All the MoSe₂ X⁰, X⁻ and X⁰/X⁻ ratio are quite homogeneous among the whole sample, indicating the absence of optical gating, charge, or energy transfer (Supplementary Figure 4 b-e). The absent interlayer interaction leads to the negligible peak shift of MoSe₂ A_{1g} mode as expected (Supplementary Figure 4f). This result confirms the FRET and optical gating scenery with 532 nm excitation from another perspective. Meantime, the interference effect from the SiO₂ substrate is ruled out by repeating the result on a transparent sapphire substrate, as detailed in Supplementary Figure 5.

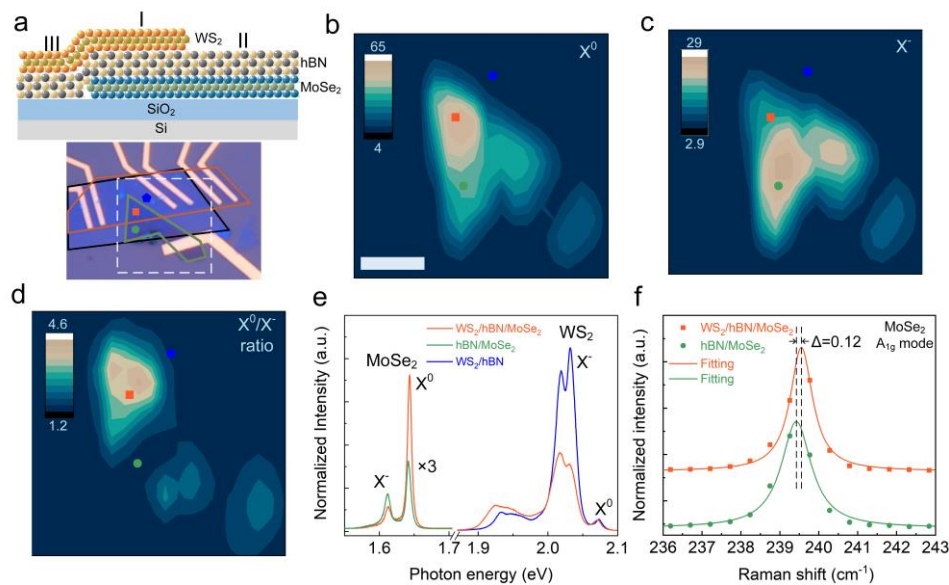


Figure 1. Sample image and optical spectroscopy of the monolayer WS₂/few-layer hBN/monolayer MoSe₂ heterojunction excited by 532 nm laser. Orange, black and green sketch denote WS₂, hBN and MoSe₂, respectively. White dashed square indicates the mapping area. Same color indication holds along this paper. a Device structure and optical image. b-d PL mapping of MoSe₂ X⁰ (b), X⁻ (c) and X⁰/X⁻ ratio (d) over the white dash square indicated in (a). e, f PL (e) and Raman (f) spectra in the corresponding sample position. The scale bar in (b) is 5 μ m.

For comparison, we fabricated another typical heterostructure device consisting of a multilayer WS_2 (~ 10 nm), hBN dielectric layer, and monolayer MoSe_2 , as presented in Figure 2a. As seen from the spectroscopy mapping excited by 532 nm laser, the MoSe_2 X^0 is quite uniform in the whole sample area, indicating no energy transfer (Figure 2b). The absence of FRET results from the negligible interaction between the indirect exciton in multilayer WS_2 and the direct exciton in monolayer MoSe_2 .^{32, 37} The significant difference from the FRET scenery in Figure 1 confirms the origin of the FRET process, *i.e.*, from the direct dipole-dipole coupling. Meanwhile, the MoSe_2 X^- emission is quenched by a factor of $\sim 3/5$ at the region I, in agreement with the photogating scenery, *i.e.*, photo-generated electrons accumulate at the WS_2/hBN interface (Figure 2c, e). The redshift of MoSe_2 A_{1g} mode is 0.2 cm^{-1} in the region I, slightly larger than 0.12 cm^{-1} in the monolayer case in Figure 1, indicating the slightly stronger p-doping effect, which results from the higher optical absorption and larger density of states in multilayer than monolayer WS_2 (Figure 2f). Similarly, the excitation wavelength was then tuned to 671 nm, which shows a negligible change of MoSe_2 X^0 emission due to the absence of FRET, as expected (Supplementary Figure 6).

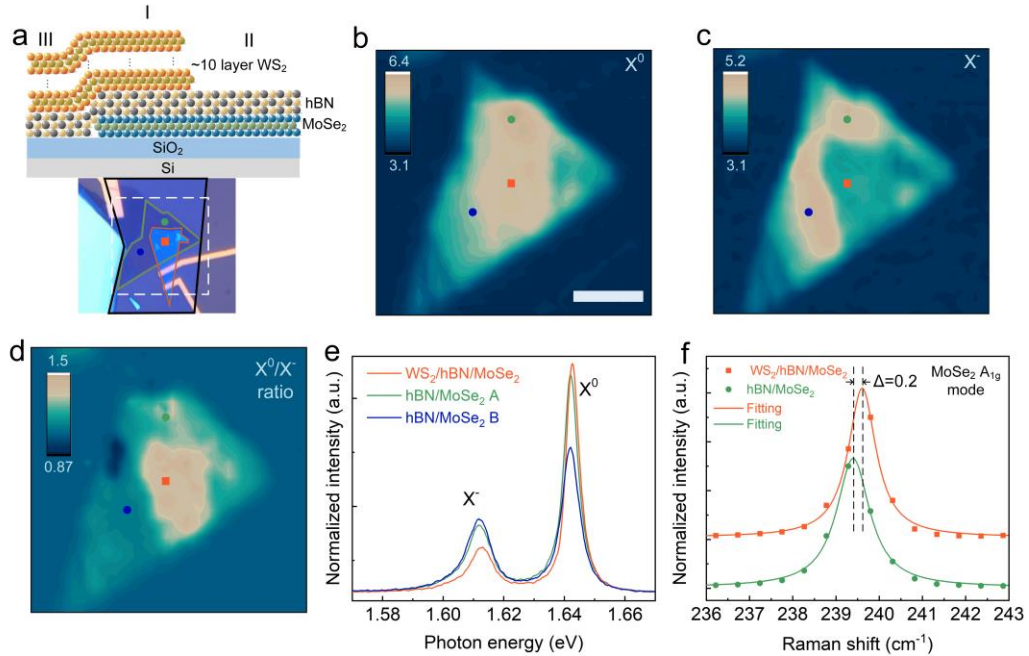


Figure 2. The sample image and optical spectroscopy of the multilayer $\text{WS}_2/\text{few-layer hBN}/\text{monolayer MoSe}_2$ heterojunction excited by 532 nm laser. a Device structure and optical image. b-d PL mapping of MoSe_2 X^0 (b), X^- (c) and X^0/X^- ratio (d) over the white dash square indicated in (a). e, f PL (e) and Raman (f) spectra in the corresponding sample position. The scale bar in (b) is 5 μm .

To understand the band alignment, which dominates the interlayer interactions in the heterojunction, we performed the electrical I - V measurement, as shown in Figure 3. The tunneling heterojunctions in the region I of Figures 1 and 2 cannot operate due to the poor conductance of TMD monolayers and the insulating hBN layer. Hence, we use the heterojunctions of monolayer WS₂/monolayer MoSe₂ and multilayer WS₂/few-layer hBN/multilayer MoSe₂ instead (Figure 3, Supplementary Figure 8). In Figure 3a, the WS₂ and MoSe₂ layers are biased and grounded, respectively. The linear scale I - V curve at different temperatures shows the typical diode characteristics, with a negative turn-on voltage and rectification ratio of $\sim 10^5$ at room temperature (Figure 3b). Since the majority carrier in both WS₂ and MoSe₂ are electrons, the negative turn-on voltage is an indicator that the conduction band (CB) of WS₂ lies above MoSe₂, in agreement with the band alignment calculated by Heyd-Scuseria-Ernzerhof (HSE06) method.³⁸ This result is also supported by the negative turn-on voltage in the I - V curve of the multilayer WS₂/few-layer hBN/multilayer MoSe₂ heterojunction (Supplementary Figure 8b). With increasing temperature, the current increases while the turn-on voltage decreases monotonously, implying the thermionic-emission-dominated transport mechanism (Supplementary Figure 9).

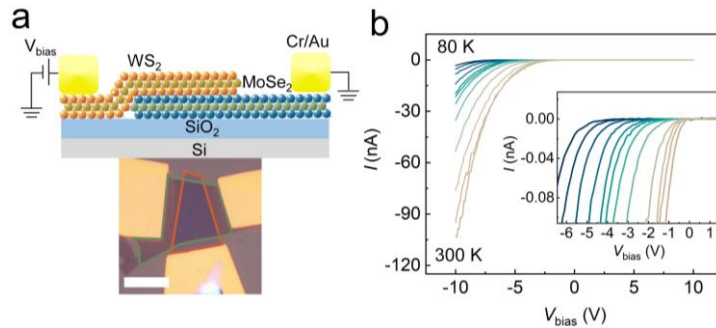


Figure 3. Electrical performance of the monolayer WS₂/monolayer MoSe₂ device. a The heterojunction device image and structure. The scale bar is 5 μ m. b Linear scale I - V performance from 80 K to 300 K with an increment of 20 K. Inset: the zoom-in image of the low bias part.

The dynamic processes in the heterojunction were evaluated by the time-resolved PL (spectral resolution ~ 2 nm), as plotted in Figure 4. The lifetime of WS₂ X⁰ (2.07 eV) on hBN, X⁻ (2.03 eV) on hBN and hBN/MoSe₂ are measured to be 13.8 ± 0.3 , 57.4 ± 0.4 , and 23.3 ± 0.5 ps, respectively, after deconvolution and fitting with a single exponential decay function $I = I_0 e^{-\frac{t}{\tau}}$ (Figure 4 a-c). It should be emphasized that the radiative recombination of exciton in the 2D system is very fast due to the small exciton Bohr radius and the large exciton optical oscillator strength, *i.e.*, in sub-

picosecond to picosecond timescale, as demonstrated in numerous theoretical and pump-probe investigations.^{34, 35, 39-41} The WS_2 X^0 lifetime approaches the temporal resolution of our testing system, as learnt from the comparison between the experimental data and the instrument response function (IRF) curve (Figure 4a). Such a short lifetime indicates that WS_2 X^0 tends to recombine radiatively rather than transfer to the acceptor. However, it should be noted that the WS_2 PL is dominated by X^- emission, which forms within ~ 2 picoseconds after exciton formation (Figure 1e)⁴². The radiative lifetime of WS_2 X^- (57.4 ± 0.4 ps) is much longer than that of the X^0 due to the difficulty for the electron dissociated from the X^- to find an unoccupied state in the band.^{34, 39} As a result, in the heterojunction, the electron-hole pair from X^- in WS_2 tends to transfer into MoSe_2 and recombine by emitting a X^0 photon. We can calculate the FRET rate ($1/\tau_{\text{FRET}}$) and efficiency (η_{FRET}) according to the formula, $1/\tau_{\text{FRET}} = 1/\tau_{\text{het}} - 1/\tau_{\text{donor}}$ and $\eta_{\text{FRET}} = 1 - \tau_{\text{het}}/\tau_{\text{donor}}$, in which τ_{donor} and τ_{het} denote the $1/e$ lifetime of the WS_2 X^- on hBN and hBN/ MoSe_2 , respectively.^{26, 43} The corresponding value τ_{FRET} is ~ 38.4 ps and η_{FRET} is 59.9%, matching well with the $\sim 50\%$ attenuation of the WS_2 X^- intensity as indicated by the steady-state PL spectra (Figure 1e). During the FRET process, the electrons dissociated from the X^- accumulate at the WS_2/hBN interface, leading to the optical gating effect as aforementioned.

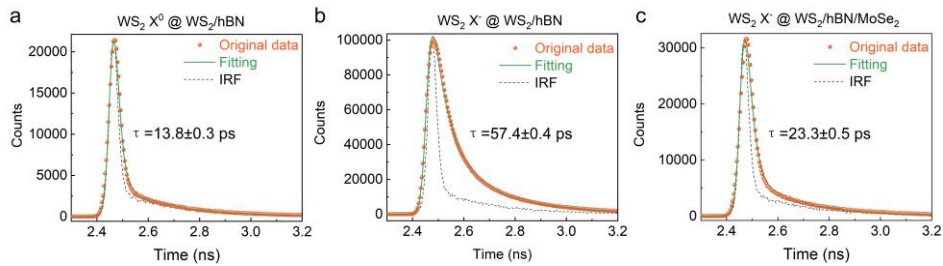


Figure 4. The time-resolved PL of WS_2 measured at 80 K. a X^0 at WS_2/hBN , b X^- at WS_2/hBN , and c X^- at $\text{WS}_2/\text{hBN}/\text{MoSe}_2$. The IRF is provided as a reference.

Besides, we used COMSOL to numerically simulate the FRET rate in monolayer $\text{WS}_2/\text{few-layer hBN}/\text{monolayer MoSe}_2$ heterojunction. We first check the exciton FRET dynamics by placing a dipole inside the WS_2 monolayer with the MoSe_2 monolayer as the absorber medium. The model and the distribution of the electric field are shown in Supplementary Figure 11. The exciton FRET

rate, $\Gamma_{X^0\text{FRET}}$, is calculated by⁴⁴⁻⁴⁶

$$\Gamma_{X^0\text{FRET}} = \frac{2}{\hbar} \frac{\text{Im}(\epsilon_{\text{MoSe}_2}(\omega_{\text{exc}}))}{4\pi} \int_{\text{MoSe}_2} \mathbf{E} \cdot \mathbf{E}^* dV \quad (1)$$

where $\epsilon_{\text{MoSe}_2}(\omega_{\text{exc}})$ is the MoSe₂ dielectric function at the exciton frequency of the WS₂, \mathbf{E} is the electric field induced by an oscillating exciton dipole $\mu e^{-i\omega_{\text{exc}}t}$ (μ is dipole moment) and the integral is taken over the MoSe₂ layer. The in-plane dipole in WS₂ has a $\mu = 13$ Debye, with other parameters shown in Supplementary Table 2.^{11, 47} Accordingly, the computed $\Gamma_{X^0\text{FRET}}$ is: $\Gamma_{X^0\text{FRET}} = 2.1 \times 10^{10} \text{ s}^{-1}$, corresponding to the FRET transfer time $\tau_{X^0\text{FRET}} = 47.6 \text{ ps}$. This value is significantly longer than WS₂ exciton lifetime (<13.8 ps) and trion formation lifetime (both lie in the range from sub-picosecond to several picoseconds)^{34, 35, 39-42}, excluding the exciton as the donor of FRET. Similarly, we check the trion ET dynamics, as detailed in Supplementary Figure 12. The estimated trion energy transfer rate $\Gamma_{X^* \text{ ET}}$ is $\Gamma_{X^* \text{ ET}} = 1.85 \times 10^{13} \text{ s}^{-1}$, corresponding to a transfer time of 0.054 ps, which is faster than the exciton FRET rate ($\Gamma_{X^0\text{FRET}} = 2.10 \times 10^{10} \text{ s}^{-1}$) and meantime shorter than the trion lifetime in WS₂ (57.4 ps). The $\Gamma_{X^* \text{ ET}}$ is faster than the value obtained experimentally (38.4 ps) due to the following reasons: 1) the trion lifetime in the heterojunction is close to the IRF, which may cause some overestimation of the lifetime, so as the underestimation of FRET rate; 2) the formula (1) was developed to estimate the exciton FRET rate, which may need a coefficient of correction in the trion ET rate calculation. Further theoretical work is required to get a deeper understanding of the underlying physics.

Based on the preceding optical spectroscopy and transport measurements, we can conclude the realistic band alignment models for three different scenarios as shown in Figure 5. The dynamics in the monolayer WS₂/hBN/monolayer MoSe₂ heterojunction include three steps, *i.e.*, (I) the formation of trions in WS₂ within ~ 2 ps on optical pumping; (II) $\sim 40.1\%$ trions recombine *via* the

recombination of electron-hole pair in the time scale of ~ 57 ps; (III) the tunneling of the dominant electron-hole pairs ($\sim 59.9\%$) into MoSe₂ *via* FRET in the time scale of ~ 38 ps (Figure 5a). The electrons generated in step (II) accumulate at the WS₂/hBN interface and serve as the photogate. In contrast, the laser excitation only induces excitons and trions in hBN/monolayer MoSe₂ (Figure 5b). In multilayer WS₂/hBN/monolayer MoSe₂, the optically generated electrons accumulate at the WS₂/hBN interface and gate the MoSe₂, leading to the exciton-dominated emission in the PL spectrum (Figure 5c).

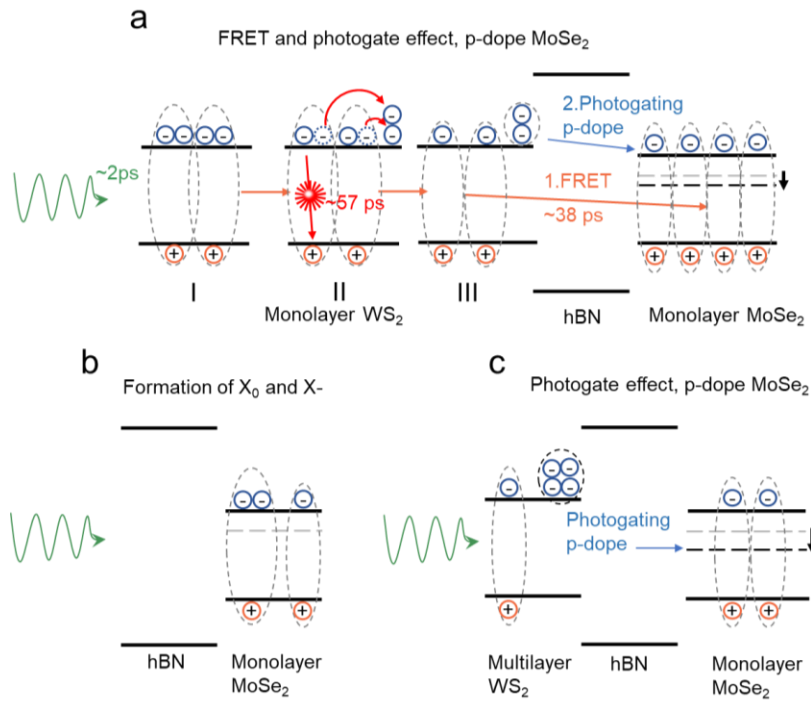


Figure 5. Schematic band diagrams and dynamic processes in different heterojunctions with above WS₂ bandgap excitation. a Monolayer WS₂/hBN/monolayer MoSe₂, b hBN/monolayer MoSe₂, c multilayer WS₂/hBN/monolayer MoSe₂. The dashed line in MoSe₂ indicates the Fermi level.

CONCLUSIONS

In conclusion, we have demonstrated a clear picture of the energy transfer dynamics in 2D WS₂/hBN/MoSe₂ heterojunction. Specifically, the dynamics are mediated by the trions, in which $\sim 59.9\%$ electron-hole pairs from the trions transfer into MoSe₂ *via* FRET channels ($\tau_{\text{FRET}} \sim 38.4$ ps) and the rest $\sim 40.1\%$ recombine by emitting photons in WS₂ ($\tau_{\text{donor}} \sim 57.4$ ps), while the extra electrons accumulate at the WS₂/hBN interface to photogate MoSe₂. These results are experimentally revealed by both the steady-state and the time-resolved optical spectroscopy and further supported by the numerical simulations. This mechanism is different from the dipole-dipole

interaction in the molecular system, and also different from the direct exciton-exciton interaction in 2D TMD heterojunctions reported to date. The understanding of the underlying physics lays the foundation for engineering the interlayer energy transfer in the 2D limit and realizing FRET-based high-performance optoelectronic devices.⁴⁸

METHODS

Sample Preparation. TMD samples are first exfoliated from bulk crystals (hq Graphene) to polydimethylsiloxane stamps and then transferred layer by layer on SiO₂ (300 nm)/Si substrate in a nitrogen-filled glovebox. A poly(methyl methacrylate) A4 (Microchem, USA) resist was spin-coated on the sample and then baked at 150 °C for 10 min. We then used a scanning electron microscope (JEOL 7001F) equipped with the nanometer pattern generation system to pattern electrodes. The exposed chip was immersed in methyl isobutyl ketone: isopropanol (3:1) mixed solution for 90 s to finalize developing. After developing, the sample was loaded into a thermal evaporator (Elite Engineering, Singapore) to deposit a Cr/Au film with a thickness of 5/50 nm. Subsequently, the chip was immersed in acetone for lift-off procedure, followed by rinsing with isopropanol and then drying with nitrogen gas. The sample was ready after a high vacuum (10⁻⁶ mbar) annealing at 200 °C for 2 hours.

Optical Spectroscopy Measurement. (1) For the absorption measurement, we used a microspectrophotometer (Craic 20) to measure the small size sample, and it is capable of measuring the sample size down to 10 μm. The spectral range can be covered from 400 to 2100 nm. (2) PL and Raman spectroscopy mapping were conducted on a spectrometer with a 800 mm focal length (Horiba-JY Evolution) equipped with a liquid nitrogen-cooled CCD detector. Samples were put in a continuous flow cryostat fixed on an xyz translation stage. The optical signals are collected by a 50× long work distance objective. All the measurements were carried out at a low temperature of 80 K with an excitation power ~10 μW. (3) The time-resolved photoluminescence spectroscopy measurement was performed with a home-built confocal micro-PL setup. Samples were also put in the cryostat operated at 80 K. A Ti: sapphire femtosecond laser with ~100 fs pulses at 80 MHz is used as the excitation source. The emission of the laser is frequency-doubled to output 400 nm

pulses and is focused ($50\times$ objective lens, $NA = 0.65$) onto the sample. The time-resolved photoluminescence emission is first spectrally resolved with a spectrometer with a focal length of 320 mm (Horiba-JY iHR320), and photons after the exit slit of the spectrometer are detected with an avalanche detector connected to a time-correlated single-photon counting module (PicoHarp 300). The excitation power is $\sim 5 \mu\text{W}$.

ACKNOWLEDGMENTS

Funding: Q.X. gratefully acknowledges the Singapore Ministry of Education Tier3 Programme “Geometrical Quantum Materials” (MOE2018-T3-1-002), AcRF Tier2 grant (MOE2017-T2-1-040), and Tier1 grant (RG 194/17). Q.X. also acknowledges strong support from Singapore National Research Foundation Competitive Research Programme “Integrated On-chip Planar Coherent Light Sources” (NRF-CRP-21-2018-0007), and National Research Foundation-Agence Nationale de la Recherche (NRF-ANR) Grant (NRF2017-NRF-ANR005 2DCHIRAL). K.W. and T.T. acknowledge support from the Elemental Strategy Initiative conducted by the MEXT, Japan, Grant Number JPMXP0112101001, JSPS KAKENHI Grant Numbers JP20H00354 and the CREST(JPMJCR15F3), JST. **Author Contributions:** Q.X. supervised the research. Z. H. conceived the idea. Z.H. and X.L. prepared the heterostructures. P.H.M. and H.V.D. performed the numerical simulation. Z.H., X.L., and M.R.A. performed the micro-spectroscopy experiments. K.W. and T.T. provided the h-BN bulk crystals. Z.H., X.L., and Q.X. analyzed the data. Z.H. wrote the manuscript with input from all authors.

ASSOCIATED CONTENT

Supporting Information Available: Absorption, Raman and PL spectra from different samples; I - V performance and fitting; PL lifetime fitting; details of numerical simulations. This material is available free of charge *via* the Internet at <http://pubs.acs.org>.

Competing interests:

The authors declare no competing interests.

REFERENCES

1. Scholes, G. D., Long-Range Resonance Energy Transfer in Molecular Systems. *Ann. Rev. Phys. Chem.* **2003**, *54*, 57-87.
2. Förster, T., Zwischenmolekulare energiewanderung und Fluoreszenz. *Annalen der physik* **1948**, *437*, 55-75.
3. Dexter, D. L., A Theory of Sensitized Luminescence in Solids. *J. Chem. Phys.* **1953**, *21*, 836-850.
4. Lu, S.; Lingley, Z.; Asano, T.; Harris, D.; Barwicz, T.; Guha, S.; Madhukar, A. J. N. I., Photocurrent Induced by Nonradiative Energy Transfer from Nanocrystal Quantum Dots to Adjacent Silicon Nanowire Conducting Channels: Toward a New Solar Cell Paradigm. *Nano Lett.* **2009**, *9*, 4548-4552.
5. Achermann, M.; Petruska, M. A.; Kos, S.; Smith, D. L.; Koleske, D. D.; Klimov, V. I., Energy-Transfer Pumping of Semiconductor Nanocrystals Using an Epitaxial Quantum Well. *Nature* **2004**, *429*, 642-646.
6. Cerdán, L.; Enciso, E.; Martín, V.; Bañuelos, J.; López-Arbeloa, I.; Costela, A.; García-Moreno, I., FRET-Assisted Laser Emission in Colloidal Suspensions of Dye-Doped Latex Nanoparticles. *Nat. Photonics* **2012**, *6*, 621-626.
7. Lyo, S. K., Energy Transfer from An Electron-Hole Plasma Layer to a Quantum Well in Semiconductor Structures. *Phys. Rev. B.* **2010**, *81*, 115303.
8. Martínez, P. L. H.; Govorov, A.; Demir, H., *Understanding and Modeling Förster-Type Resonance Energy Transfer (FRET): FRET from Single Donor to Single Acceptor and Assemblies of Acceptors*; Springer; Singapore, **2017**, Vol. 2, pp 18-21.
9. Wang, Q. H.; Kalantar-Zadeh, K.; Kis, A.; Coleman, J. N.; Strano, M. S., Electronics and Optoelectronics of Two-Dimensional Transition Metal Dichalcogenides. *Nat. Nanotechnol.* **2012**, *7*, 699-712.
10. Hu, Z.; Wu, Z.; Han, C.; He, J.; Ni, Z.; Chen, W., Two-Dimensional Transition Metal Dichalcogenides: Interface and Defect Engineering. *Chem. Soc. Rev.* **2018**, *47*, 3100-3128.
11. Chernikov, A.; Berkelbach, T. C.; Hill, H. M.; Rigosi, A.; Li, Y.; Aslan, O. B.; Reichman, D. R.; Hybertsen, M. S.; Heinz, T. F., Exciton Binding Energy and Nonhydrogenic Rydberg Series in Monolayer WS₂. *Phys. Rev. Lett.* **2014**, *113*, 076802.
12. You, Y.; Zhang, X.-X.; Berkelbach, T. C.; Hybertsen, M. S.; Reichman, D. R.; Heinz, T. F., Observation of Biexcitons in Monolayer WSe₂. *Nat. Phys.* **2015**, *11*, 477-481.
13. Mak, K. F.; He, K.; Lee, C.; Lee, G. H.; Hone, J.; Heinz, T. F.; Shan, J., Tightly Bound Trions in Monolayer MoS₂. *Nat. Mater.* **2013**, *12*, 207-211.
14. Xiao, D.; Liu, G. B.; Feng, W.; Xu, X.; Yao, W., Coupled Spin and Valley Physics in Monolayers of MoS₂ and Other Group-VI Dichalcogenides. *Phys. Rev. Lett.* **2012**, *108*, 196802.
15. Schaibley, J. R.; Yu, H.; Clark, G.; Rivera, P.; Ross, J. S.; Seyler, K. L.; Yao, W.; Xu, X., Valleytronics in 2D Materials. *Nat. Rev. Mater.* **2016**, *1*, 1-15.
16. Hong, X.; Kim, J.; Shi, S. F.; Zhang, Y.; Jin, C.; Sun, Y.; Tongay, S.; Wu, J.; Zhang, Y.; Wang, F., Ultrafast Charge Transfer in Atomically Thin MoS₂/WS₂ Heterostructures. *Nat. Nanotechnol.* **2014**, *9*, 682-686.
17. Xu, W.; Liu, W.; Schmidt, J. F.; Zhao, W.; Lu, X.; Raab, T.; Diederichs, C.; Gao, W.; Seletskiy, D. V.; Xiong, Q., Correlated Fluorescence Blinking in Two-Dimensional Semiconductor Heterostructures. *Nature* **2017**, *541*, 62-67.
18. Kim, J.; Jin, C.; Chen, B.; Cai, H.; Zhao, T.; Lee, P.; Kahn, S.; Watanabe, K.;

Taniguchi, T.; Tongay, S., Observation of Ultralong Valley Lifetime in WSe₂/MoS₂ Heterostructures. *Sci. Adv.* **2017**, *3*, e1700518.

19. Du, W.; Zhao, J.; Zhao, W.; Zhang, S.; Xu, H.; Xiong, Q., Ultrafast Modulation of Exciton-Plasmon Coupling in a Monolayer WS₂-Ag Nanodisk Hybrid System. *ACS Photonics* **2019**, *6*, 2832-2840.

20. Wen, X.; Xu, W.; Zhao, W.; Khurgin, J. B.; Xiong, Q., Plasmonic Hot Carriers-Controlled Second Harmonic Generation in WSe₂ Bilayers. *Nano Lett.* **2018**, *18*, 1686-1692.

21. Long, R.; Prezhdo, O. V., Quantum Coherence Facilitates Efficient Charge Separation at a MoS₂/MoSe₂ van der Waals Junction. *Nano letters* **2016**, *16*, 1996-2003.

22. Rivera, P.; Schaibley, J. R.; Jones, A. M.; Ross, J. S.; Wu, S.; Aivazian, G.; Klement, P.; Seyler, K.; Clark, G.; Ghimire, N. J.; Yan, J.; Mandrus, D. G.; Yao, W.; Xu, X., Observation of Long-Lived Interlayer Excitons in Monolayer MoSe₂-WSe₂ Heterostructures. *Nat. Commun.* **2015**, *6*, 6242.

23. Rivera, P.; Seyler, K. L.; Yu, H.; Schaibley, J. R.; Yan, J.; Mandrus, D. G.; Yao, W.; Xu, X., Valley-Polarized Exciton Dynamics in a 2D semiconductor Heterostructure. *Science* **2016**, *351*, 688-691.

24. Zang, H.; Routh, P. K.; Huang, Y.; Chen, J. S.; Sutter, E.; Sutter, P.; Cotlet, M., Nonradiative Energy Transfer from Individual CdSe/ZnS Quantum Dots to Single-Layer and Few-Layer Tin Disulfide. *ACS Nano* **2016**, *10*, 4790-4796.

25. Raja, A.; Montoya Castillo, A.; Zultak, J.; Zhang, X. X.; Ye, Z.; Roquelet, C.; Chenet, D. A.; van der Zande, A. M.; Huang, P.; Jockusch, S.; Hone, J.; Reichman, D. R.; Brus, L. E.; Heinz, T. F., Energy Transfer from Quantum Dots to Graphene and MoS₂: The Role of Absorption and Screening in Two-Dimensional Materials. *Nano Lett.* **2016**, *16*, 2328-2333.

26. Prins, F.; Goodman, A. J.; Tisdale, W. A., Reduced Dielectric Screening and Enhanced Energy Transfer in Single- and Few-layer MoS₂. *Nano Lett.* **2014**, *14*, 6087-6091.

27. Liu, Y.; Li, H.; Zheng, X.; Cheng, X.; Jiang, T., Giant Photoluminescence Enhancement in Monolayer WS₂ by Energy Transfer from CsPbBr₃ Quantum Dots. *Optic. Mater. Exp.* **2017**, *7*, 1327.

28. Zhang, L.; Sharma, A.; Zhu, Y.; Zhang, Y.; Wang, B.; Dong, M.; Nguyen, H. T.; Wang, Z.; Wen, B.; Cao, Y.; Liu, B.; Sun, X.; Yang, J.; Li, Z.; Kar, A.; Shi, Y.; Macdonald, D.; Yu, Z.; Wang, X.; Lu, Y., Efficient and Layer-Dependent Exciton Pumping across Atomically Thin Organic-Inorganic Type-I Heterostructures. *Adv. Mater.* **2018**, *30*, No. e1803986.

29. Froehlicher, G.; Lorchat, E.; Berciaud, S., Charge *Versus* Energy Transfer in Atomically Thin Graphene-Transition Metal Dichalcogenide van der Waals Heterostructures. *Phys. Rev. X* **2018**, *8*, 011007.

30. Liu, X.; Pei, J.; Hu, Z.; Zhao, W.; Liu, S.; Amara, M. R.; Watanabe, K.; Taniguchi, T.; Zhang, H.; Xiong, Q., Manipulating Charge and Energy Transfer between 2D Atomic Layers *via* Heterostructure Engineering. *Nano Lett.* **2020**, *20*, 5359-5366.

31. Kozawa, D.; Carvalho, A.; Verzhbitskiy, I.; Giustiniano, F.; Miyauchi, Y.; Mouri, S.; Castro Neto, A. H.; Matsuda, K.; Eda, G., Evidence for Fast Interlayer Energy Transfer in MoSe₂/WS₂ Heterostructures. *Nano Lett.* **2016**, *16*, 4087-4093.

32. Wu, L.; Chen, Y.; Zhou, H.; Zhu, H., Ultrafast Energy Transfer of Both Bright and Dark Excitons in 2D van der Waals Heterostructures Beyond Dipolar Coupling. *ACS Nano* **2019**, *13*, 2341-2348.

33. Xu, W.; Kozawa, D.; Liu, Y.; Sheng, Y.; Wei, K.; Koman, V. B.; Wang, S.; Wang, X.;

- Jiang, T.; Strano, M. S.; Warner, J. H., Determining the Optimized Interlayer Separation Distance in Vertical Stacked 2D WS₂: hBN: MoS₂ Heterostructures for Exciton Energy Transfer. *Small* **2018**, *14*, No. e1703727.
34. Zhao, J.; Zhao, W.; Du, W.; Su, R.; Xiong, Q., Dynamics of Exciton Energy Renormalization in Monolayer Transition Metal Disulfides. *Nano Res.* **2020**, 1-8.
35. Robert, C.; Lagarde, D.; Cadiz, F.; Wang, G.; Lassagne, B.; Amand, T.; Balocchi, A.; Renucci, P.; Tongay, S.; Urbaszek, B.; Marie, X., Exciton Radiative Lifetime in Transition Metal Dichalcogenide Monolayers. *Phys. Rev. B.* **2016**, *93*, 205423.
36. Chakraborty, B.; Bera, A.; Muthu, D. V. S.; Bhowmick, S.; Waghmare, U. V.; Sood, A. K., Symmetry-Dependent Phonon Renormalization in Monolayer MoS₂ Transistor. *Phys. Rev. B.* **2012**, *85*, 161403.
37. Stavola, M.; Dexter, D. L.; Knox, R. S., Electron-Hole Pair Excitation in Semiconductors via Energy Transfer from An External Sensitizer. *Phys. Rev. B.* **1985**, *31*, 2277-2289.
38. Kang, J.; Tongay, S.; Zhou, J.; Li, J.; Wu, J., Band Offsets and Heterostructures of Two-Dimensional Semiconductors. *Appl. Phys. Lett.* **2013**, *102*, 012111.
39. Wang, H.; Zhang, C.; Chan, W.; Manolatu, C.; Tiwari, S.; Rana, F., Radiative Lifetimes of Excitons and Trions in Monolayers of the Metal Dichalcogenide MoS₂. *Phys. Rev. B.* **2016**, *93*, 045407.
40. Palumbo, M.; Bernardi, M.; Grossman, J. C., Exciton Radiative Lifetimes in Two-Dimensional Transition Metal Dichalcogenides. *Nano Lett.* **2015**, *15*, 2794-2800.
41. Poellmann, C.; Steinleitner, P.; Leierseder, U.; Nagler, P.; Plechinger, G.; Porer, M.; Bratschitsch, R.; Schuller, C.; Korn, T.; Huber, R., Resonant Internal Quantum Transitions and Femtosecond Radiative Decay of Excitons in Monolayer WSe₂. *Nat. Mater.* **2015**, *14*, 889-893.
42. Singh, A.; Moody, G.; Tran, K.; Scott, M. E.; Overbeck, V.; Berghäuser, G.; Schaibley, J.; Seifert, E. J.; Pleskot, D.; Gabor, N. M.; Yan, J.; Mandrus, D. G.; Richter, M.; Malic, E.; Xu, X.; Li, X., Trion Formation Dynamics in Monolayer Transition Metal Dichalcogenides. *Phys. Rev. B.* **2016**, *93*, 041401.
43. Sampat, S.; Guo, T.; Zhang, K.; Robinson, J. A.; Ghosh, Y.; Acharya, K. P.; Htoon, H.; Hollingsworth, J. A.; Gartstein, Y. N.; Malko, A. V., Exciton and Trion Energy Transfer from Giant Semiconductor Nanocrystals to MoS₂ Monolayers. *ACS Photonics* **2016**, *3*, 708-715.
44. Govorov, A. O.; Carmeli, I., Hybrid Structures Composed of Photosynthetic System and Metal Nanoparticles: Plasmon Enhancement Effect. *Nano Lett.* **2007**, *7*, 620-625.
45. Hernández-Martínez, P. L.; Govorov, A. O., Exciton Energy Transfer between Nanoparticles and Nanowires. *Phys. Rev. B.* **2008**, *78*, 035314.
46. Hernández-Martínez, P. L.; Govorov, A. O.; Demir, H. V., Generalized Theory of Forster-Type Nonradiative Energy Transfer in Nanostructures with Mixed Dimensionality. *J. Phys. Chem. C.* **2013**, *117*, 10203-10212.
47. Feierabend, M.; Berghäuser, G.; Selig, M.; Brem, S.; Shegai, T.; Eigler, S.; Malic, E., Molecule Signatures in Photoluminescence Spectra of Transition Metal Dichalcogenides. *Phys. Rev. Mater.* **2018**, *2*, 014004.
48. Kim, J.; Kim, H.-R.; Lee, H.-C.; Kim, K.-H.; Hwang, M.-S.; Lee, J. M.; Jeong, K.-Y.; Park, H.-G., Photon-Triggered Current Generation in Chemically-Synthesized Silicon Nanowires. *Nano Lett.* **2019**, *19*, 1269-1274.

For the table of contents only:

